A MOLECULAR PARTNERSHIP BETWEEN CEP290 AND SANS AFFECTS THE FUNCTION OF PRIMARY CILIA IN BODY AXIS DEVELOPMENT

by

JOE CULBERT

A THESIS

Presented to the Department of Biology
and the Robert D. Clark Honors College
in partial fulfillment of the requirements for the degree of
Bachelor of Science

June 2020

An Abstract of the Thesis of

Joe Culbert for the degree of Bachelor of Arts
in the Department of Biology to be taken June 2020

Title: A molecular partnership between Cep290 and Sans affects the function of primary cilia in body axis development

Approved: _____*Jennifer B. Phillips*_____
Primary Thesis Advisor

Usher syndrome is the most common cause of hereditary deaf-blindness. The most severe type of Usher syndrome, type 1 (USH1), can be caused by mutations in any one of 7 genes. Individuals with USH1 are born deaf and have progressive vision loss. One of the seven causative USH1 genes, *USH1G*, encodes the protein Ush1g. This thesis will refer to the gene *USH1G* as *SANS*, and the protein Ush1g as Sans because of the previous works describing them as such. Sans has many protein interaction domains, enabling it to act as a scaffold for assembling multiple proteins in the same cellular location. Research conducted by our collaborators sought to identify proteins that physically interact with Sans. Using a particular domain of Sans as “bait”, they detected an interaction with the protein Cep290. Cep290 has been implicated in a range of disorders involving cellular structures called primary cilia. Cilia influence the flow of fluids through tissues or organs, including the flow of cerebrospinal fluid, and are involved in the transport of molecules between distinct parts of the cell. Diseases resulting from genetic defects in the formation or function of cilia are known collectively as ciliopathies.

Previous research in the Westerfield lab investigated how the Sans-Cep290 interactions in zebrafish affect cilia function in eyes. The Westerfield lab had previously generated and characterized zebrafish *sans* mutations that resulted in vision loss, hearing impairment and balance defects within the first week of life, consistent with a model of Usher syndrome. The *sans* gene in zebrafish is duplicated, named *sansa* and *sansb*. To investigate the interaction between Sans and Cep290, the Westerfield lab used the existing *sans* mutant lines to observe whether simultaneous impairment of the zebrafish *cep290* gene would have a greater impact on zebrafish vision than defects in *sans* alone. While collecting these data, a body axis curvature was observed in the young fish with this double impairment. Because previous work with zebrafish deficient *sans* had not shown this characteristic, the curvature was hypothesized to be a result of the new *cep290* mutation.

For my thesis research, I collected additional data on the compensatory relationship between zebrafish *sans* genes, characterized the novel *cep290* mutation and designed experiments to investigate the Cep290-Sans interaction in tissues related to body axis regulation. To assess how the two zebrafish *sans* genes work in conjunction to replace one another in the event that one is non-functional, we examined gene expression during a range of timepoints within the first week of life, and observed that in the absence of one functional *sans* gene, the level of expression of the other increases. To determine the cause of the body axis curvature observed in the *sans;cep290* double mutants, we used selective breeding to segregate the *cep290* mutation from the *sans* mutations and then conducted genetic crosses of *cep290* mutant carriers to observe the body axis development of the offspring. We found that *cep290*

single mutants had normal body axis development through the first week of life, but observed a spinal curvature at a later juvenile stage in these fish.

We investigated the exact timing of the late spinal curvature and calculated the standard length of *cep290* mutant zebrafish offspring exhibiting the first signs of the defect, and performed a skeletal staining experiment on these fish to visualize the spinal deformities. We next tested the effect of mother's genotype on the timing of the body axis curvature in *cep290* mutants. Although *cep290* mutants from mothers with functional copies of *cep290* were able to avoid early body axis defects, offspring from *cep290* mutant mothers exhibited a range of early ciliopathy defects, including body axis curvature. Finally, we observed the expression of *sansb* and *cep290* in wild-type fish at the stage of embryonic development in which the long body axis is forming, a process regulated by the coordinated movements of cilia within a structure called Kupffer's vesicle (KV). We found that both genes are expressed in the region of KV in zebrafish embryos, and thus are present in the right place to play a role in this process. These experiments collectively support the hypothesis that the Sans-Cep290 relationship influences body axis development in addition to retinal function related to USH.

Acknowledgements

I would like to thank Professor Prikryl for sparking my interest in Molecular Biology and advising me in the steps to join a lab.

I would also like to thank my Thesis Committee. My primary advisor, Jennifer Phillips, has been with me through every step in the creation of this thesis. She pushed me to be the best I could and ensured I was on the same page when it came to the experiments. This thesis couldn't have been possible without her. Thank you to my second reader, Monte Westerfield, who offered me the opportunity to work in his lab as an undergraduate to develop this thesis. Finally, thank you to my CHC Representative and CHC Professor, Mark Carey, who has helped me in my writing capabilities and provided great writing advice for future papers and this thesis. Thank you again, without my Thesis Committee this project could not have been possible.

I would also like to thank Tom and Susan Luten for their help in putting me through college. Without them I would not have been able to attend such a wonderful university and had the chance to work in an amazing research lab.

Finally, I would like to thank my mom, Stacy, and my girlfriend, Noelle. My mom always gave me great advice and helped to calm me down when I needed it. Noelle has been there for me since the beginning of my college career and has always helped me deal with the challenges and stress of school and the thesis process.

Table of Contents

1 Introduction 1

1.1 Usher Syndrome (USH) 1

1.2 Cilia and Ciliopathies 3

1.3 Zebrafish as a Model Organism 4

1.4 Sans (USH1g) 6

1.5 Cep290 7

1.6 Thesis Reasoning 9

2. Materials and Methods 12

2.1 Husbandry 12

2.2 Reverse Transcription-PCR 13

2.3 Maternal Contribution of Cep290 15

2.4 Standard Length 15

2.5 Analysis of images from live animals 16

2.6 Plasmid Preparation 16

2.7 RNA Probe Synthesis 20

2.8 In-situ Hybridization 22

2.9 Alcian Alizarin Double Stain to Visualize Skeletal Elements 25

3. Results 27

3.1 *sansb* appears to be upregulated in the absence of *sansa* 27

3.2 Defining and analyzing the onset of late spinal curvature in *cep290* mutant larvae 28

3.3 Maternal contribution of *cep290* ensures normal early body axis patterning 31

3.4 A timeline of developmental requirements for Cep290 and Sans in body axis regulation 34

3.5 *sansb* and *cep290* colocalize in the region of Kupffer's vesicle 36

4. Conclusion and Discussion 38

5. Future Studies 42

Bibliography 45

List of Figures

Figure 1: Ciliopathies impact numerous organs and systems 4

Figure 2: Sans interacts with Cep290 in vitro via the CENT domain 7

Figure 3: A time course of *sans* expression during embryonic and larval development 28

Figure 4: Skeletal staining reveals the orientation of the delayed spinal curvatures 30

Figure 5. Lack of maternal contribution results in variable body axis defects 33

Figure 6. Cep290 and Sans importance in zebrafish body axis development 35

Figure 7: *sansb* and *cep290* are expressed in the tail bud proximal to the Kupffer's vesicle 37

List of Tables

Table 1: RT-PCR Mix 14
Table 2: PCR Mix 15
Table 3: Ligation Mixture 17
Table 4: Probe Synthesis Mix 21
Table 5: Percentage of mutant offspring in each category of curvatures 34

1 Introduction

1.1 Usher Syndrome (USH)

Usher syndrome (USH), named for Scottish Ophthalmologist Charles Usher, is the most common cause of combined deaf-blindness. USH, a genetic disorder that affects 1 out of 6000 people (Kimberling et al., 2010), is characterized by vision and hearing defects, sometimes accompanied by balance dysfunction (Mathur & Yang, 2014). Based on the severity and age of onset of these symptoms, Usher syndrome is classified into three clinical categories (USH 1-3). The most severe type, USH1, classifies patients as having deafness from birth, vision loss beginning in first decade of life, and an abnormal or absent balance response (Kremer et al., 2006; Espinós et al., 1998). USH2, the most common, is described as having moderate to severe hearing loss at birth with gradual vision loss detectable after the first decade of life (Dona et al., 2018; Reisser et al., 2002). USH3 is characterized by gradual hearing loss, variable balance defects and onset of vision loss detectable after the second decade of life (Dad et al., 2009; Mathur & Yang, 2014).

Early diagnosis of USH is critical for optimal management and monitoring of the symptoms. Research into USH helps physicians offer more information about the disorder. Affected individuals and their families will have the chance to put all possible accommodations in place to further educational and psychosocial success and prepare for the progressive symptoms (Kimberling et al., 2010; Mathur and Yang, 2014).

More than a dozen different genes have been linked to Usher syndrome (Kimberling et al., 2010; Reiners et al., 2006). Genes contain the information to make proteins, which in turn perform a variety of cellular functions. Genetic mutations alter

the protein-coding information, leading to loss of or abnormal protein function that manifests as disease symptoms. The specific cells affected by the loss of USH gene function, and the resulting disruption of the encoded USH proteins, are the mechanosensory hair cells of the inner ear responsible for balance and hearing, and the light-sensing photoreceptor cells of the retina (Kremer et al., 2006). USH1 pathology results from the most severe dysfunction and degeneration of these cells.

Thus far, 7 genes have been identified as causative of USH1. The proteins encoded by these genes interact with each other, creating protein complexes that are responsible for maintaining vision and hearing. In the retina, the USH protein complexes are thought to function in loading molecular cargo onto the connecting cilium of the photoreceptors for transport (Reiners et al., 2006). The symptoms that result from disruption of this cilia-related function have led to USH being classified as a ciliopathy.

Animal models such as mouse and zebrafish have been instrumental in identifying the roles of USH genes in vision and hearing (Kremer et al., 2006; Dona et al., 2018). Mouse models of USH1 all display hearing and balance deficits, but relatively few exhibit a retinal phenotype (Reniers et al., 2006). Zebrafish models have added to our knowledge of the roles of USH genes in hearing and balance, as well as providing models for the retinal disorders seen in USH (Seiler et al., 2005; Phillips et al., 2011, Phillips et al., 2015).

Research into Usher syndrome is essential to understand better the molecular interactions involved in the tissues affected in this disorder. Furthermore, most USH genes are expressed broadly throughout other tissues in the body, such as in the brain

and gut, which suggests potential roles of these genes outside of sensory cells. Research into these genes will help demystify the complexity of genetic diseases, including the category of diseases known as ciliopathies.

1.2 Cilia and Ciliopathies

Because of the evidence suggesting that vision loss in USH is due at least in part to disrupted function at the connecting cilium of photoreceptors, it is often classified as a ciliopathy—an extensive category of human diseases caused by dysfunction of the cilia. Cilia are microscopic hair like structures that are found in many cells of the body (Fliegauf et al., 2007). Cilia are composed of cable-like assemblies of proteins, called microtubules, surrounded by a membrane. Cilia fall into two categories, motile and non-motile, or primary, cilia (Reiter & Leroux, 2017). Primary cilia function in conducting signals from the environment or from cell to cell and are involved in protein trafficking, whereas motile cilia function in propelling cells and fluid flow. The coordinated beating of motile cilia regulates the movement of fluid, such as cerebrospinal fluid (CSF). This fluid flow is important in embryonic patterning, including body axis development (Hirokawa et al., 2006; Okada et al., 2005; Grimes et al., 2016).

There are many proteins involved with the structure, maintenance, and function of cilia. A mutation in any of the genes that code for these proteins leads to defective cilia that in turn result in diseases of various ciliated organs and tissues, known collectively as ciliopathies (Fig. 1). Ciliopathies range from global, affecting many ciliated tissues and organs, to restrictive, only affecting one or few tissues. Since global ciliopathies affect multiple tissues and organs, they are more severe and are potentially lethal (Fliegauf et al., 2007). By contrast, USH proteins localize to the connecting

cilium of photoreceptors in the eyes, but no other ciliary functions for USH proteins have been described to date, classifying USH as a restrictive ciliopathy (Kremer et al., 2006; Soursch et al., 2014; Reiners et al., 2006).

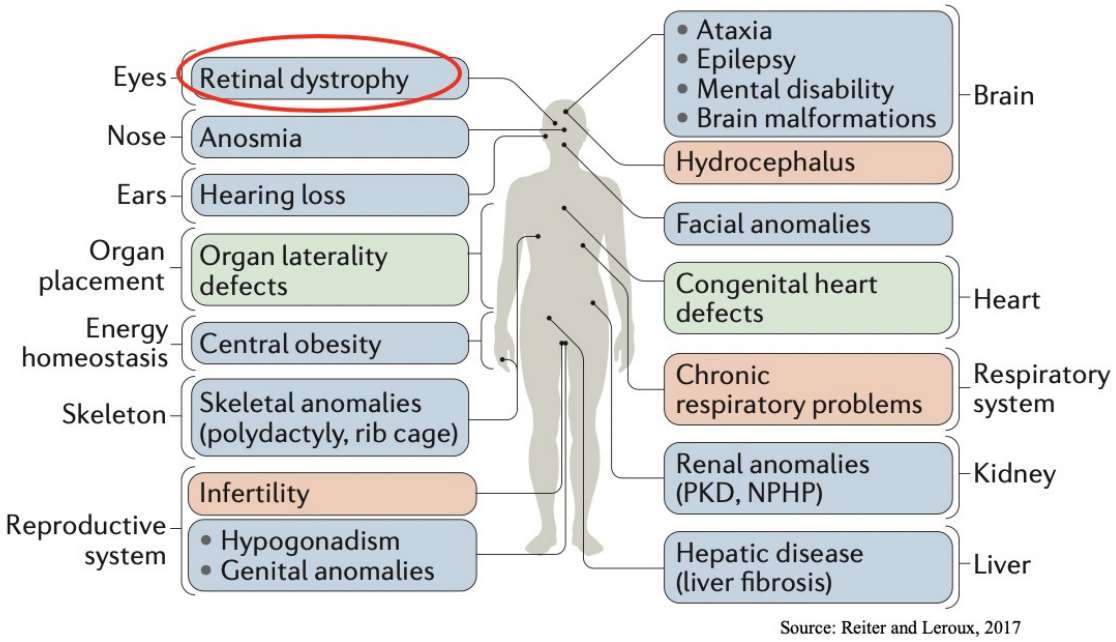

Figure 1: Ciliopathies impact numerous organs and systems

The figure shows organs and tissues that can be affected by ciliopathies. Ciliopathies can be global, having multiple tissues and organs affected, or restrictive, affecting only one or a couple tissues or organs. The red oval indicates the symptoms of USH, showing a restrictive ciliopathy. Source: Reiter and Leroux, 2017

1.3 Zebrafish as a Model Organism

Zebrafish develop rapidly, reaching a free-swimming larval stage with functional tissues and organ systems by 5 days post-fertilization, and sexual maturity at three months. Zebrafish lay large numbers of fertilized eggs in a single mating, which are also transparent during early growth making the developmental processes easy to observe. The quick development allows researchers to study disease mechanisms and validate the effect of developing therapies on zebrafish that mimic the mutant

phenotypes of a human disorder (Phillips and Westerfield, 2014). Zebrafish and human genomes are more than 70% similar overall, and genes corresponding to 82% of known human disease genes can be found in zebrafish (Howe et al., 2013). Zebrafish have been used to examine many genetic factors that underlie human disease, including USH. Zebrafish models of USH1 have abnormal swimming patterns observable at 5 days old and do not respond to tapping stimulus, indicating dysfunctions in hearing and balance (Söllner et al., 2004; Seiler et al, 2005; Phillips et al., 2011; Phillips et al., 2015). USH1 proteins are responsible for maintaining the proper shape and function of structures in the mechanosensory hair cells of the inner ear. Examination of the hair cells in these zebrafish models shows malformation of these structures, which directly causes the observed hearing and balance defects. Eye reflex tracking and electrophysiological tests on zebrafish reveal further defects in animals lacking functional USH proteins, and this dysfunction is accompanied by degeneration of photoreceptor cells (Seiler et al., 2005; Phillips et al., 2011; Dona et al., 2018).

The zebrafish model of USH1F, caused by mutations in the *PCDH15* gene, was also informative in understanding how duplicated zebrafish genes share functional roles (Seiler et al., 2005). In about 25% of cases, zebrafish have two functional genes where there is only a single corresponding gene in humans (Force et al., 1999). In the case of PCDH15, one of the zebrafish genes, *pcdh15a*, functions primarily in the ear, where the other, *pcdh15b*, is important in retinal cell function. *pcdh15a* mutant zebrafish have severe balance and hearing defects but no visual dysfunction, whereas temporary depletion of *pcdh15b* produced significant visual defects.

Another disorder that has been more recently investigated using zebrafish is idiopathic scoliosis (IS). IS is characterized by spinal curvatures that can lead to disfigurement, pain, limited mobility, and in severe cases heart and lung problems (Grimes et al., 2016). Mutations in genes associated with IS are shown to cause motile cilia dysfunction, causing defects in cerebrospinal fluid (CSF) flow in both humans and zebrafish (Hayes et al., 2014; Grimes et al., 2016). Recently, genome sequencing in a group of patients with IS identified variants in a number of different cilia-related genes, including several USH genes, which have not been previously linked to scoliosis (Baschal et al., 2018). This thesis will explore the potential role of the USH gene, *sans*, in contributing to the developmental events that pattern the body axis, disruptions of which could influence symptoms of scoliosis.

1.4 Sans (USH1g)

Sans is the protein encoded by the USH gene *SANS* (Weil et al., 2003; Kremer et al., 2006; Reiners et al., 2006). Sans protein localizes to the hair bundles of the inner ears and the connecting cilium of the photoreceptors of the eyes (Soursch et al., 2019; Caberlotto et al., 2011). Sans is composed of several different protein-protein binding motifs, including ankyrin repeats, a sterile alpha motif, a PDZ binding motif, and the central (CENT) domain (Soursch et al., 2019; Weil et al., 2003). These binding motifs tether the components of the USH complex together, classifying it as a scaffold protein. (Weil et al., 2003; Yan et al., 2010).

Two genes corresponding to the human SANS gene are found in zebrafish, *sansa* and *sansb* (Phillips et al., 2015). *sansa* and *sansb* have overlapping expression in ear and retinal cells of young fish, and single mutations in either gene do not result in

USH symptoms, suggesting functional redundancy. The overlapping function of zebrafish *sans* genes is in contrast to the divided function observed zebrafish USH1F genes *pcdh15a* and *pcdh15b*, which have largely split the roles of this gene in the development and maintenance of sensory cells (Seiler et al., 2005).

To understand more about Sans function, our collaborators Nasrin Soursch and Uwe Wolfrum recently investigated the CENT domain of Sans, using it as bait to detect potential interactions with other proteins biochemically. One of the newly discovered interactions with the CENT domain of Sans, summarized in Figure 2, was with Cep290. The interaction between Sans and Cep290 was confirmed by performing the reverse experiment, using the domain of Cep290, indicated by the green oval in Figure 2, as bait to bind to Sans.

This interaction was the basis for an ongoing collaboration with the Westerfield lab to study the interaction in our already existing *sans* mutants.

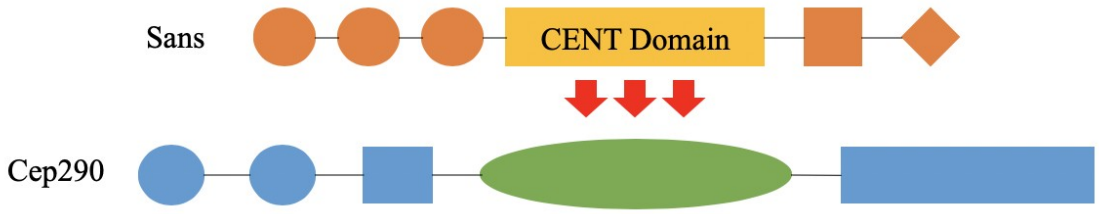

Figure 2: Sans interacts with Cep290 in vitro via the CENT domain

Recent work by our collaborators has revealed that the CENT domain of Sans interacts with a region within the central domain of Cep290, indicated by the green oval. The Westerfield lab has been testing whether this protein interaction results in a genetic interaction using the zebrafish model.

1.5 Cep290

Cep290 is a large, multidomain protein that has been found to function in microtubule transport and localizes in the connecting cilium of photoreceptors as well

as centrosomes of dividing cells (Baye et al., 2011; Chang et al., 2006). Centrosomes assemble large arrays of microtubules into a structure called the spindle that aids in cell division during development or tissue proliferation (Frank et al., 2008). Mutations in the *CEP290* gene have been implicated in multiple ciliopathies that vary in symptoms and severity, sometimes acting in a restricted fashion, affecting one organ, other times affecting a broad range of organs. Examples of the variability of diseases caused by *CEP290* mutations include Leber congenital amaurosis (LCA), Meckel-Gruber syndrome, and Joubert syndrome (Craige et al., 2010). LCA is a disorder that causes blindness due to a disruption in protein transport along the connecting cilium in photoreceptors (den Hollander et al., 2008). Joubert syndrome is characterized as a group of disorders that cause vision loss and defects in the brain that lead to other abnormalities such as loss of control of body movements and breathing (Valente et al., 2006). The brain malformations and vision loss are both consistent with ciliopathies. Meckel-Gruber syndrome affects many tissues and organs, such as the liver, kidneys, and brain, all of which depend on cilia for proper development and function. The most common symptoms include abnormal growths or sacs in the covering of the brain, malformations in the kidneys and liver during fetal development, and the presence of extra fingers or toes (Frank et al., 2008). Survival beyond birth is unlikely in individuals with Meckel-Gruber syndrome.

A temporary loss of function of *cep290* in zebrafish results in a variety of phenotypes including hydrocephalus, small eyes, kidney cysts, and, most notably for this thesis, a body curvature (Baye et al., 2011). A study that was published during my thesis research on the *cep290* mutation also reported a body axis curvature in adult

cep290 mutants (Lessieur et al., 2019). Body curvature during the first week of life is a common characteristic of cilia dysfunction in zebrafish (Zaghloul and Katsanis, 2011). The curvature observed in these ciliopathy mutants is most likely due to defects in the ciliary movement that regulates CSF flow down the spinal cord. CSF bidirectional flow is important in the maintenance and development of the body axis (Okada et al., 2005; Grimes et al., 2016).

A previous study investigating temporary loss of function of *cep290* in zebrafish described vision impairment and protein transport defects, and the clinical symptoms of humans with *CEP290* mutations indicate the importance of Cep290 in cilia development and ciliary transport of proteins (Baye et al., 2011; Craige et al., 2010; Change et al., 2006). The *cep290* mutant described in this thesis was generated in the Westerfield lab specifically to study the Sans-Cep290 interaction.

1.6 Thesis Reasoning

The Westerfield lab previously characterized zebrafish *sans* function in hearing and vision, generating mutations in *sansa* and *sansb* to observe the symptoms, or phenotypes, resulting from loss of function (Phillips et al., 2015). Single mutants, *sansa* or *sansb*, appeared to see and hear normally when evaluated in the first week of life, but *sansa;sansb* double mutants displayed vision impairment along with hearing and balance defects observable by 5 days post fertilization (dpf).

These sans mutants were subsequently used in collaboration with the Wolfrum group to validate the Sans-Cep290 interaction in an animal model. *cep290* mutations targeted to the region involved in interactions with the Sans CENT domain were introduced into the *sans* double mutant background, producing *sansa;sanb;cep290*

triple mutant lines. A previous student in the Westerfield lab studied these fish to see whether zebrafish visual function would be adversely affected in triple mutants beyond that which had been previously observed in the *sansa;sanb* double mutants.

While generating these fish for analysis, the researchers observed that the mutant offspring displayed a curved body axis by 5 dpf. This pronounced developmental defect was hypothesized to be an effect of the *cep290* mutation, because body axis curvature is a hallmark of other ciliopathy mutants in zebrafish and no such phenotype had been observed in the *sans* mutants prior to the introduction the *cep290* mutation. To test this hypothesis, fish carrying *cep290* and *sans* mutations were mated to genetically normal, wild-type fish. The resulting offspring carried subsets of the original mutations such that the *cep290* mutations segregated away from the *sans* mutations in some animals. When these *cep290* carriers were bred to produce offspring with *cep290* mutations, no body axis curvature was seen at 5 dpf. Given the body axis defect seen in young fish in which *cep290* and *sans* genes were simultaneously disrupted, this result suggested that *sans* genes may play a role in cilia function beyond the retina.

Thus, as a result of investigating the interactive relationship between Cep290 and Sans in visual function, we have discovered a novel interaction in which it appears Sans may play a role in modifying the activity of Cep290 in regulating the function of primary cilia in body axis development. This thesis will test the hypothesis that the effects of *cep290* depletion on cilia-dependent body axis patterning is enhanced by the simultaneous absence of *sans* function. As part of addressing this hypothesis, it was necessary to collect additional data on the individual genetic mutations. First, because

functional redundancy of the zebrafish *sans* genes was inferred based on the previous analysis, I performed an experiment to confirm the molecular basis of this genetic compensation. Next, given that the *cep290* mutation in this study was generated in the *sans* mutant background and had not been evaluated on its own, characterization of phenotype was necessary to compare with the findings in the triple mutant.

Previous zebrafish studies have helped develop a better understanding of the molecular mechanisms involved in Usher syndrome. Further characterization of *sans* and *cep290* will contribute to our body of knowledge as to how USH genes interact in other cellular processes. Adding to our understanding of the genetic basis of disease provides increased information and support for individuals living with USH, as well as the physicians who manage their care. The extent to which USH genes may be linked to other disorders such as scoliosis remains to be determined, but an expanded understanding of USH protein function and the molecular interactions they participate in, can lead to improved clinical tools. In the realm of genetic diagnosis, for example, determining the likely result of a newly discovered mutation in a known disease gene can provide higher quality information to both patient and doctor on which decisions about disease management options, candidacy for emerging therapeutic interventions, and family planning may be based. Likewise, precise knowledge of essential protein function in all relevant tissues and developmental timepoints can help to target new gene therapies to the appropriate cells while minimizing risk of side effects. The results described in this thesis are part of a global research effort to enhance our collective understanding of the genetic variations that influence virtually every aspect of human life.

2. Materials and Methods

2.1 Husbandry

Zebrafish were raised in the University of Oregon zebrafish facility in a 10 hour dark and 14 hour light cycle. All experiments performed on zebrafish were carried out with stringent oversight and compliance with all University of Oregon's Institutional Care and Use Committee mandates. Zebrafish mutations of *sansa, sansb,* and *cep290* were generated using gene editing, TALENS for *sansa and sansb* and CRISPR for *cep290*. Adult zebrafish carrying the desired genetic mutations were set up in crossing tanks, which include an outer box, an inner screen, and an optional divider used to regulate breeding time. Strips of netting that simulate river grass were used for environmental enrichment to promote mating behavior. Zebrafish normally spawn at the beginning of the light cycle. The male zebrafish swim alongside the female which stimulates her to release eggs, the male releases his sperm into the water to fertilize the eggs, which drop below the inner screen, out of reach of the adult zebrafish. Once embryos were observable at the bottom of the crossing cage, the adult fish were transferred into a new outer box filled with water. The eggs in the original outer box were collected by pouring the water into a tea strainer with a mesh diameter smaller than the eggs. The eggs were then transferred to a clean Petri dish with fish water. The embryos were selected and separated from nonviable eggs and debris. The selected eggs were placed in Embryo Medium (EM). EM is a mixture of NaCl, KCl, $CaCl_2 \cdot 2H_2O$, $MgSO_4 \cdot 7H_2O$, methylene blue, and fish water. The embryos were cleaned daily to remove debris and add fresh EM and raised until the desired stage. Embryos raised

beyond one week of age were moved to the nursery tanks where the fish were fed multiple times a day with regular water changes.

2.2 Reverse Transcription-PCR

Reverse Transcription polymerase chain reaction (RT-PCR) was performed to analyze RNA expression in *sans* single mutants. The steps taken were in accordance to the manufacturer's instructions of the RT-PCR kit (ThermoFisher). 10 embryos per sample were euthanized by rapid cooling before being flash-frozen at -80°C to preserve RNA integrity prior to processing. RNA was extracted from frozen embryos using 250 μl of Trizol-Reagent per sample. Trizol-Reagent isolates RNA, DNA, and proteins. The samples were homogenized using an electric pestle.

The samples were incubated at room temperature for 5 minutes before adding 50 μl of Chloroform. Chloroform facilitated the separation of the solution into phases. The solution was allowed to incubate for 5 minutes at room temperature. The samples were spun on the centrifuge at 12,000 rotations per minute (rpm) for 15 minutes at 4°C, this helped further separate the phases. The aqueous phase of each sample, the watery layer containing the RNA, was removed to a new tube. 125 μl of isopropyl alcohol was added to the separated aqueous phase to precipitate the RNA and separate it from the aqueous solution. The samples were incubated at room temperature for 10 minutes and then spun in the centrifuge at 12,000 rpm for 10 minutes at 4°C. After precipitation and centrifugation, the RNA formed a white pellet at the bottom of the tube. 70% ethanol was added to the pellet and then centrifuged at 7,600 rpm for 5 minutes at 4°C. Ethanol cleans the salts out of the precipitate. After removing the ethanol, the pellet was allowed

to air dry at 37˚C. 25 μl of 1:10 EDTA and RNase-free water solution was added to wash the pellet.

0.5 μl of Oligo(dT)s and 0.5 μl of 10 mM dNTP mix were added to 4 μl of sample solution, which facilitated the first steps of complementary DNA (cDNA) synthesis. The solutions were incubated at 65˚C for 5 minutes and then put on ice. Next, RT-PCR mix was added to each tube (Table 1). The solutions were then incubated for 1 hour at 50˚C, then for 5 minutes at 85˚C and then put on ice.

Reagent	**Volume**
RT-Buffer (10X)	1 μl
$MgCl_2$ (25 mM)	2 μl
DTT (0.1 M)	1 μl
Supercript III (40 U/ μl)	0.5 μl
RNaseOUT (200 U/ μl)	0.5 μl
Total	**5 μl**

Table 1: RT-PCR Mix

1 μl of RNase H was added to the solutions and then incubated at 37˚C for 20 minutes. RNase H digests the excess RNA, resulting in purified cDNA. 0.7 μl of the cDNA was used in PCR using the mix in Table 2. cDNA is used because it is more stable and easier to work with during the amplification steps. The PCR program entered into the thermocycler generates repeated cycles of temperature changes that facilitate DNA denaturing, annealing of the primers to the template, and elongation of the new DNA strands. The time of the elongation cycle was altered based on length (number of base pairs) of the desired PCR product. The PCR products were visualized on a 2% agarose gel made with SYBRSafe DNA Gel Stain (ThermoFisher), which was run for about 10 minutes at 150 volts. The gel was then imaged using a Digital Gel Imaging System The Gel Doc XR+.

Reagent	Concentration	Volume
2X PCR Mix	1X	6 μl
Forward Primer	0.2 μM	0.25 μl
Reverse Primer	0.2 μM	0.25 μl
dH_2O		5.5 μl
Total		**12 μl**

Table 2: PCR Mix

2.3 Maternal Contribution of Cep290

Zebrafish mating pairs were chosen to produce the desired offspring genotypes, which included *cep290* mutant females and heterozygous *cep290* females. Wild-type zebrafish controls were also raised to compare with the mutant crosses. About 200 embryos were analyzed.

Offspring that displayed an early curvature at 3 dpf were separated and photographed using a dissecting microscope fixed with a camera.

2.4 Standard Length

Offspring from *cep290* carriers were raised in the nursery for several weeks. Body axes were observed from day 15-22. Each day, the offspring were recorded using a cell phone camera in their tanks over a piece of graph paper with known grid dimensions. About 200 fish were analyzed for this procedure.

2.5 Analysis of images from live animals

Still images were analyzed using the ImageJ image processing software. The mutant offspring along with the wild-type control offspring were measured for their

body axis bending angles. The angle was measured in a straight line back from the tip of the offspring's mouth to the distal end of the uniform bend, excluding any change in direction at the tip of the tail. Mutants were categorized by the degree of bending.

The recorded videos of older larvae were observed to detect the first signs of bending in the offspring. The length of each individual fish displaying the bend was measured using the grid of 7 mm squares. These measurements were recorded, and the average standard length and standard deviation were calculated using Excel equation shortcuts.

2.6 Plasmid Preparation

RNA probes for *sansa*, *sansb*, and *cep290* were prepared to be used in in-situ hybridizations. The gene fragments used in the following ligation step were amplified by PCR using specific primers for *sansa*, *sansb*, and *cep290*, respectively, from 92 hours post fertilization (hpf) wild-type cDNA generated in the previous RT-PCR experiment (section 2.3). The mixture described in Table 3 was used for ligation of the prepared cDNA into plasmids. The plasmids are circularized pieces of DNA engineered to accept DNA fragments up to a certain size. The DNA code of the plasmid includes several antibiotic resistance genes, base sequences required to facilitate enzymatic reactions that cut the DNA strand, and sites to promote PCR amplification of select regions of the plasmid.

Reagent	**Volume**
cDNA	0.5-4 μl
Salt solution	1 μl
Water	Add to total 5 μl
pCR™II-Blunt-TOPO®*	1 μl
Total	**6 μl**

Table 3: Ligation Mixture

* Plasmid provided by ThermoFisher Scientific, Waltham, MA. USA

This reaction mix was incubated for 5 minutes at room temperature, then transferred to ice. These conditions promote the splicing of the gene-specific fragment into the plasmid vector, creating circular DNA strands containing the inserted gene fragments

12 μl of competent bacterial cells (ThermoFisher) were added to a 1.7 ml Eppendorf tube. The competent cells were engineered to incorporate foreign DNA when the cell walls are permeabilized. 0.2 μl of the ligation mixture was added to the competent cells. This mixture was kept on ice while a heat block was warmed to 42°C. Once the heat block reached 42°C, the competent cells with the plasmid were placed in the heat block for 30 seconds. This increase in heat alters the bacterial cell walls to allow the insert-containing plasmids to be taken up into the cells. After 30 seconds the mixture was returned to the ice. 100 μl of SOC broth was added to the tube. SOC broth is a nutrient-rich broth used to grow bacterial cells. The tubes were incubated at 37°C for 1 hour on the shaker. 1 ml of the SOC broth with bacterial growth was placed on plates of LB media, a broth used to grow liquid cultures of bacteria, prepared with the antibiotic kanamycin. The plasmid used in the ligation step carries a kanamycin resistance gene, which allows it to grow in the presence of kanamycin, whereas bacteria without this antibiotic resistance conferred by the plasmid will not propagate. Beads were placed on the plate and swirled around to inoculate the entire plate. The plates were placed in a 37°C room overnight.

After growing overnight, individual colonies from these plates were removed with a sterile toothpick and used to inoculate 5 ml of LB media in glass test tubes mixed

with kanamycin at a 1:4000 dilution. The cultures were incubated at 37°C overnight in the shaker. The cultures were retrieved from the shaker, poured into centrifuge tubes, and spun for 20 seconds at 14,000 rpm. The supernatant was removed, and the process was repeated three times until a large pellet of bacterial cells was collected. The supernatant was removed carefully to avoid contamination. 250 μl of Buffer PI (Qiagen) was added to each pellet. Buffer PI is a resuspension buffer used to dislodge the pellets from the bottom of the tubes. The tubes were dragged along a rigid, bumpy surface to agitate and resuspend the pellet.

After about 5 minutes, 250 μl of Buffer P2 (Qiagen) was added to each tube. Buffer P2 is a lysis buffer used to break open the cells containing the plasmid. The tubes were inverted multiple times until a blue precipitate was seen. The blue color is caused by a chemical reaction between bacterial cell contents and the P2 solution, and signifies that cell lysis is occurring.

After another 5 minutes for the lysis process to complete, 350 μl of Buffer N3 (Qiagen) was added to each tube. Buffer N3 is a neutralization buffer that precipitates cellular debris, allowing only nucleic acids, including the plasmid, to be suspended in the aqueous solution. The tubes were spun at 4°C for 10 minutes at 14,000 rpm.

Each supernatant was poured into a purification tube, which contained a filter that binds the plasmid DNA while allowing salts and other substances to pass through. The tubes were spun at 24°C for 3 minutes at 3,000 rpm and then for 10 seconds at 5,000 rpm.

700 μl of Buffer PE (Qiagen) was added to each purification tube. Buffer PE, which contains ethanol, is a wash buffer used to clean plasmids of any impurities. The

tubes were spun for 10 seconds at 5,000 rpm. The columns were transferred to new collection tubes and spun again for 1 minute at 14,000 rpm.

The purification columns were placed in collection tubes and 25 μl of Buffer EB (Qiagen) was added directly to each filter. Buffer EB is an elution buffer that releases the plasmid from the filter. After the mixtures sat for 2 minutes, they were spun for 30 seconds at 10,000 rpm. Another 25 μl of Buffer EB was added to each tube, and again after 2 minutes the mixtures were spun for 30 seconds at 10,000 rpm. This product yielded the plasmids plus inserts, suspended in liquid buffer.

Excess volume of the overnight liquid cultures for each selected colony were used to make a glycerol stock. 500 μl of LB culture was placed into an Eppendorf tube with 1 ml of glycerol, mixed and stored at -80°C. This was done to preserve a source of plasmids containing the desired cDNA insert for future experiments.

2.7 RNA Probe Synthesis

15 μl of water, 10 μl of plasmid, 3 μl restriction enzyme buffer 3.1, and 2 μl of restriction enzyme were mixed together to linearize each plasmid. This step is to facilitate the subsequent process of synthesizing an antisense RNA probe from the gene fragment incorporated into the plasmid. 70 μl of water was added to 30 μl of each linearized plasmid solution. 500 μl of Buffer PB (Qiagen) was added to a purification column followed immediately by the water plasmid mixes. This buffer washes the linearized plasmids of the excess material. The purification columns were spun for 4 minutes at 3,000 rpm. The excess was discarded into guanidine waste, and tubes were spun again for 15 seconds at 5,000 rpm.

The purification columns were fitted with a fresh collection tube. 700 μl of Buffer PE was added to the column and spun for 30 seconds at 5,000 rpm. Buffer PE is a wash buffer that rids the linearized plasmid of impurities. A new collection tube was added to each purification column and spun for 1 minute at 14,000 rpm. The purification columns were then placed in 1.7 ml Eppendorf tubes. 40 μl of Buffer EB was added to release the plasmid from the filter and into solution. After 4 minutes the tubes were spun for 30 seconds at 10,000 rpm. The end product yields a linearized DNA template that serves as a guide for the synthesis of the complementary RNA strand that will be used as an RNA probe for in-situ hybridization.

The probe synthesis mixture (ThermoFisher) described in Table 4 was used to generate the RNA probe.

Reagent	**Volume**
10X Transcription Buffer	2 μl
10X Nucleotide Mix (DIG)	2 μl
DTT (0.1 M)	1 μl
RNase Inhibitor*	1 μl
SP6 or T7 RNA Polymerase*†	1 μl
DNA Template	8 μl
H_2O	5 μl
Total	**20 μl**

Table 4: Probe Synthesis Mix

* Marks an enzyme which should be kept on ice

† Use the polymerase that gives you antisense plasmids (3’ → 5’)

The nucleotide mix included in the probe synthesis mix contains nucleotides (the building blocks of nucleic acids) tagged with digoxigenin (DIG). These tags enable the probe to be detected by an antibody binding reaction in a subsequent step, described below.

This mixture was incubated for 2 hours at 37°C to allow the RNA polymerase to transcribe RNA probes from the DNA template. 1 μl of DNAse was added to the mixture and allowed to incubate at 37°C for 5 minutes. DNAse digests the DNA template without degrading the RNA probes.

The probes were then purified using purification columns. 80 μl of nuclease-free water was added to the mixtures to bring the volume to roughly 100 μl. 350 μl of RTL buffer (Qiagen) and 250 μl of ethanol were added to break up any residual template and wash the probe. The mixtures were immediately spun at 3,000 rpm for 4 minutes. The flow through was disposed in the Trizol waste.

500 μl of RPE buffer (Qiagen) was added to each purification column. RPE functions as a wash buffer to clean salts away. The tubes were spun for 1 minute at 3,000 rpm and the purification columns were transferred to new tubes and spun again for 1 minute at 14,000 rpm to remove any excess RPE buffer. This step was repeated a second time to ensure pure probes.

50 μl of Elution Buffer (Qiagen) was added to each tube and allowed to sit for 3 minutes before it was spun at 10,000 rpm for 20 seconds, allowing the purified probes to release from the filter and into the flow through liquid. 95 μl of pre-hybridization solution was added to the eluted probes to stabilize the RNA for storage.

2.8 In-situ Hybridization

Hybridization is the term used to describe the action of the RNA probe binding to complementary portions of native RNA. Embryos were collected and euthanized before being immersed in 4% Paraformaldehyde (PFA diluted in Phosphate Buffered Saline containing .01% Tween-20 (PBS-T)) at 4°C overnight, which preserves the

embryos at their developmental stages. About 10 embryos at 16 hpf were used for each RNA probe prepared. The fixed embryos were washed twice in PBS-T for 5 minutes each to remove the PFA, then washed in 100% methanol for 10 minutes. This dehydrates the tissue so that it can be stored in the freezer without forming ice crystals, which can disrupt the cellular integrity preserved by the earlier fixation step. Once dehydrated, the embryos can be stored in 100% methanol at -20 ˚C for months until needed. To proceed with the in situ hybridization, the embryos were rehydrated with gradually decreasing concentrations of methanol to PBS-T. Embryos were transferred from the 100% methanol to 66% methanol in 33% PBS-T, followed by a wash of 33% methanol in 66% PBS-T. Two subsequent washes of 100% PBS-T followed. All washes were performed for 5 minutes on the shaker. PBS-T is a washing buffer that cleans the methanol off of the embryos, the increasing concentration of PBS-T to methanol gradually rehydrates the embryos from their dehydrated state.

Embryos were incubated in Pre-hybridization solution (pre-hyb) for one hour at 65˚C. Pre-hyb is a blocking solution that reduces nonspecific binding and protein-protein interactions and increases the quality of the probe signal at the end of the process. The embryos were then transferred to hybridization mix (RNA probe diluted 1:100 in pre-hyb) pre-heated to 65˚C. Hybridization mix is made up of pre-hyb containing the RNA probe complementary to the RNA transcript of interest. The embryos were hybridized overnight at 65˚C. This temperature is ideal for the hybridization of the RNA probe to the respective gene transcript because it is a permissive temperature for hydrogen bonding between paired nucleic acids, but

stringent enough that there is a low probability of mismatched base pairing that would result in non-specific binding of the probe to other RNAs.

After hybridization, a series of washes were performed at 65˚C. Each solution for these washes was prewarmed to 65ºC. The washes started with 66% pre-hyb to 33% 2X saline-sodium citrate (SSC), followed by 33% pre-hyb to 66% 2X SSC followed by a 100% 2X SSC wash for 5 minutes each. 2X SCC is a detergent used to control the pH of the solution and help preserve the RNA bond to its complementary sequence in the zebrafish cells and wash away other non-specifically bound probe. The tissue was washed with 0.2X SSC followed by two washes with 0.05X SSC for 20 minutes each. The decreasing concentrations of SSC are used to further control the pH of solution.

The next washes were performed at room temperature (RT) for 5 minutes each on a shaker. The washes were performed with gradually decreasing concentration of 0.05X SSC to PBS-T, starting with 66% 0.05X SSC to 33% PBS-T followed with a 33% 0.05X SSC to 66% PBS-T. The third wash was performed in 100% PBS-T. The decreasing concentrations of 0.05X SSC to PBS-T washes the embryos of the 0.05X SSC to avoid mixing the SSC with the following washes.

After these washes, the embryos were treated with blocking solution (PBS-T, 2% sheep serum and 0.2% BSA) for 1 hour at RT on a shaker. Blocking solution helps to prevent background caused by nonspecific binding of antibodies. Embryos were then incubated overnight in anti-digoxigenin (dig) (Roche) antibody diluted 1:5000 in blocking solution at 4˚C on the shaker. The anti-digoxigenin antibody binds to the DIG labeled nucleotides incorporated into the RNA probe.

A series of 5 washes with PBS-T for 5, 10, and 3x 15 minutes were performed on a shaker. These PBS-T washes clean the embryos of excess antibody and blocking solution. After these washes, a wash with colorization buffer (100 nm Tris-HCl, 50 mM $MgCl_2$, 100 mM NaCl, 0.1% Tween-20, sterile water) for 5 minutes was performed to acclimate the tissue to the higher pH of colorization solution. The samples were then treated with a colorization mix (45 μl nitro-blue tetrazolium (NBT) stock and 35 μl 5-bromo-4-chloro-3-indolyl phosphate (BCIP) stock diluted in 10 ml of colorization buffer) (Roche) until a reaction pigment was visible. NBT and BCIP react with the anti-digoxigenin antibody to create a blue/purple pigment that corresponds to the location of the RNA transcript of interest.

2.9 Alcian Alizarin Double Stain to Visualize Skeletal Elements

This staining was performed to visualize the orientation and location of the spinal curvatures in *cep290* mutant fish. Alcian blue binds strongly to large molecules in cartilage, whereas Alizarin Red binds to positively charged metals, like calcium in the bone.

All of the following steps, with the exception of the bleach step, were performed on the shaker at room temperature. 10 fish were first euthanized and then fixed in 2% PFA/1X PBS for 1 hour followed by a 10 minute wash in 50% ethanol to prepare the tissue for the ethanol-based staining solution.

The double stain was performed overnight by immersing the samples in a mixture of Alcian premix (0.04% Alcian Blue/10mM $MgCl_2$/80% ethanol) with 0.5% Alizarin Red Stock. The mixture was made by adding 20 μl of Alizarin Red Stock for every 1 ml of premix.

Following the overnight stain, the fish were washed with 80% ethanol/10mM $MgCl_2$ for one hour. The fish were then rinsed with 50% ethanol followed by a 25% ethanol rinse, both for 5 minutes each.

The fish were exposed to 3% H_2O_2/0.5% KOH for 10 minutes in the fume hood. Potassium hydroxide (KOH) is a caustic base and should be handled with extreme care. KOH is used to break down soft tissues and clear pigment from the embryos to allow visualization of bone stains. This step was not performed on the shaker.

To remove excess staining chemicals not bound to the skeletal tissue, the samples were transferred to a 25% glycerol/0.1% KOH mix and checked every 15 minutes until red pigment was observed seeping from the tissue, which indicated the Alizarin stain beginning to dissociate from the bones. The fish were then immersed in 50% glycerol/0.1% KOH overnight and a fresh solution of 50% glycerol/0.1% KOH was added the following day for short term storage.

The stained fish were imaged using a dissecting microscope with a mounted camera. Lateral, ventral, and dorsal views were captured to observe the orientation of the spinal curvature.

3. Results

3.1 *sansb* appears to be upregulated in the absence of *sansa*

Previous results in our lab showed single *sansa* or *sansb* mutants appearing normal, but *sansa;sansb* double mutants presenting vision loss with hearing and balance defects. This presented the hypothesis that single *sans* mutant fish could compensate for the absence of one mutated gene by increasing the activity of the duplicate gene. This experiment was designed to detect increased activity by visualizing the abundance of *sans* transcript at several stages of development in wild-type and mutant backgrounds. cDNA was synthesized from *sansa* mutants and wild-type controls and expression of *sansa* and *sansb* genes were analyzed by RT-PCR (Figure 3).

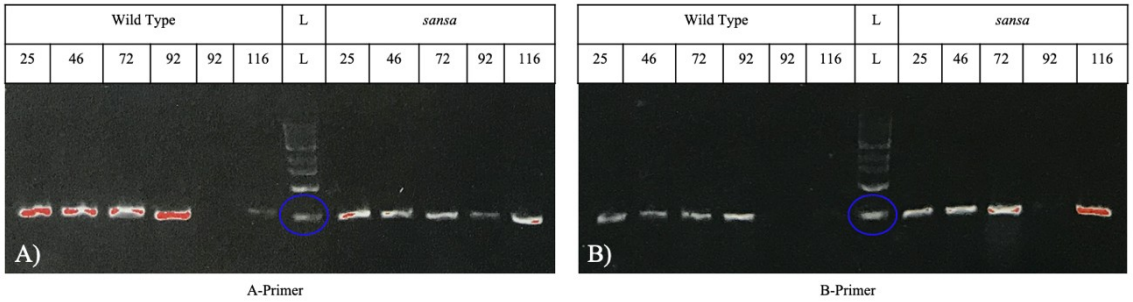

Figure 3: A time course of *sans* expression during embryonic and larval development

Stage matched wild-type zebrafish serve as a control and the ladder, represented as L, provides a reference for the size of the amplified PCR fragments. The closest ladder band, marked with a blue circle, is 500 base pairs (bp). The sansa and sansb PCR fragments were anticipated to be between 400-500 bp. The A-primer was used to detect the expression of *sansa* in wild-type and *sansa* mutants (A). Levels of *sansa* expression appeared consistent over this five day time course in both wild type and *sansa* mutants. The B-primer was used to detect the expression of *sansb* in wild-type and *sansa* mutants (B). The result shows that although *sansb* expression levels do not vary through all timepoints examined in wild type, expression appears to be increasing over time in the *sansa* mutant tissue.

The gel shows the expression of *sansb* being upregulated in *sansa* mutants. This provides evidence of genetic compensation in the single *sansa* mutants. The reciprocal experiment, detecting *sansa* transcript levels in *sansb* mutants, was not completed due to the Covid-19 lab shutdown.

3.2 Defining and analyzing the onset of late spinal curvature in *cep290* mutant larvae

A previous student in the Westerfield lab observed body axis curvature at 5 dpf when studying *sansa;sansb;cep290* triple mutants. When the *cep290* mutation was removed from the *sans* background through selective breeding, the body axis in *cep290*

single mutants was normal at 5dpf, but a pronounced body axis curvature was noted in juvenile and young adult fish.

As part of the effort to characterize the phenotype of this new *cep290* mutant, we sought to identify the developmental timepoint in which *cep290* is required for proper body axis maintenance.

We first investigated this developmental event by defining its onset based on Standard Length (SL) measurements. Throughout the first week of life, developmental timepoints in zebrafish raised with standard methods are invariant. However, after this first week, variation in nutritional uptake and other fitness factors uncouples the correlation between growth and age. To estimate the developmental milestones of zebrafish after this stage in development accurately, researchers routinely use SL rather than age (Parichy et al., 2011).

Embryos derived from matings between carriers of the *cep290* mutation were raised with standard conditions for 2 weeks. From day 15 onward they were observed so that the length of fish when they first developed the late spinal curvatures could be pinpointed. A body length of 7.4 mm $\pm$ 0.48 mm was identified as the stage at which the first spinal deformities could be observed.

A double stain was performed on wild-type fish and their *cep290* mutant siblings to analyze the orientation of spinal curvatures. The cartilage was stained blue and the bone was stained red/purple.

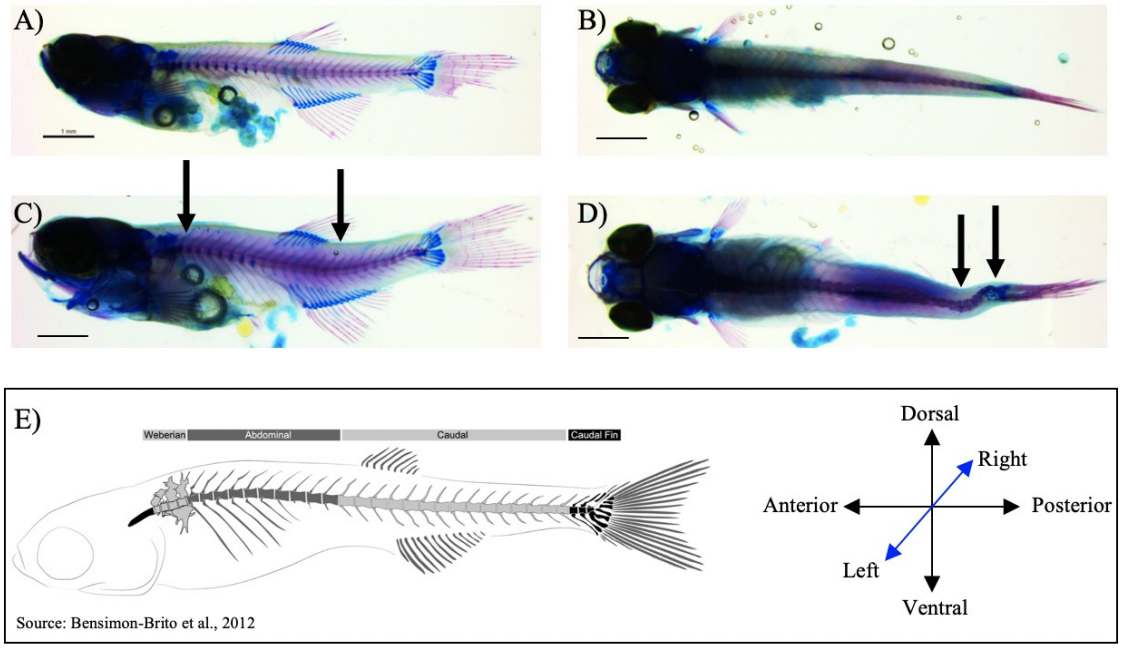

Figure 4: Skeletal staining reveals the orientation of the delayed spinal curvatures

The bone and cartilage stains for wild-type (A and B) and *cep290* mutant (C and D) were compared to visualize the orientation of the spinal curvature. *cep290* mutants have multiple bends occurring along the spine. Frame E showcases the figure used to describe the position of the spinal curvatures with an accompanying compass to help orient to the dimensions of fish anatomy. The blue arrow of the compass represents a lateral plane. The black bar scales 1 mm. Source of Frame E Figure: Bensimon-Brito et al., 2012

Analysis of the skeletal elements revealed multiple curves in the spines of *cep290* mutants. A pronounced dorsal arch was observed in the abdominal vertebrae just posterior to the Weberian structure, and a ventral dip in the caudal vertebrae is detected at the level of the anal fin (Fig. 4.C). Mutants also displayed lateral displacements of the caudal vertebrae anterior to the tail (Fig. 4.D). 100% of the fish with this spinal curvature phenotype were identified by sequence analysis as *cep290* mutants. The spinal curvatures detected are consistent with those observed in a *cep290* mutant study that was published during our analysis of our *cep290* mutant (Lessieur et al., 2019). The

mutation in *cep290* reported in that publication affects approximately the same region as the mutation generated in our lab, suggesting that the resulting truncated protein may also have impaired Sans binding.

Young fish with combined *cep290* and *sans* mutations exhibit an earlier curvature than the single *cep290* mutants, suggesting that there is an earlier developmental timepoint at which *cep290* is important for body axis regulation. Because this early defect was not detected in our observations of offspring derived from parents carrying one mutant copy of the *cep290* gene, we hypothesized that the early requirement may be met by contributions from the maternal effect. We tested this hypothesis to characterize the molecular cause of the delayed spinal curvature further.

3.3 Maternal contribution of *cep290* ensures normal early body axis patterning

The mother's genotype is a major contributor to the outcome of early zebrafish development. Yolks of the eggs are preloaded with maternal transcripts and proteins, which are used in numerous developmental events before the embryo's own genes are active. Analyzing this 'maternal contribution' helps to determine when certain proteins are required for developmental milestones.

To assess whether spinal curvatures seen in *cep290* mutant offspring with heterozygous *cep290* mothers were delayed due to maternal contributions of *cep290* that were functional earlier in development, we observed body axis formation in embryos from *cep290* homozygous mutant mothers compared with those from *cep290* heterozygous mothers.

We found that the majority of offspring of *cep290* mutant mothers, which lack functional *cep290* transcripts in the yolk, displayed pronounced body axis curvatures by

3 dpf, whereas mutant offspring of heterozygous *cep290* mutant mothers were confirmed to have normal body axes at this stage. This supports the conclusion that the maternal contribution of *cep290* transcripts from heterozygous mothers is enough to rescue the mutant offspring from body axis defects early in embryonic development. We hypothesize that simultaneously depleting *sans* along with *cep290* limits the rescue effect of the maternal contribution and results in an earlier body axis deformity.

Because there was significant variation in the degree of the body axis curvature, we defined categories based on the angle of curvature relative to the anterior-posterior plane (Fig. 5).

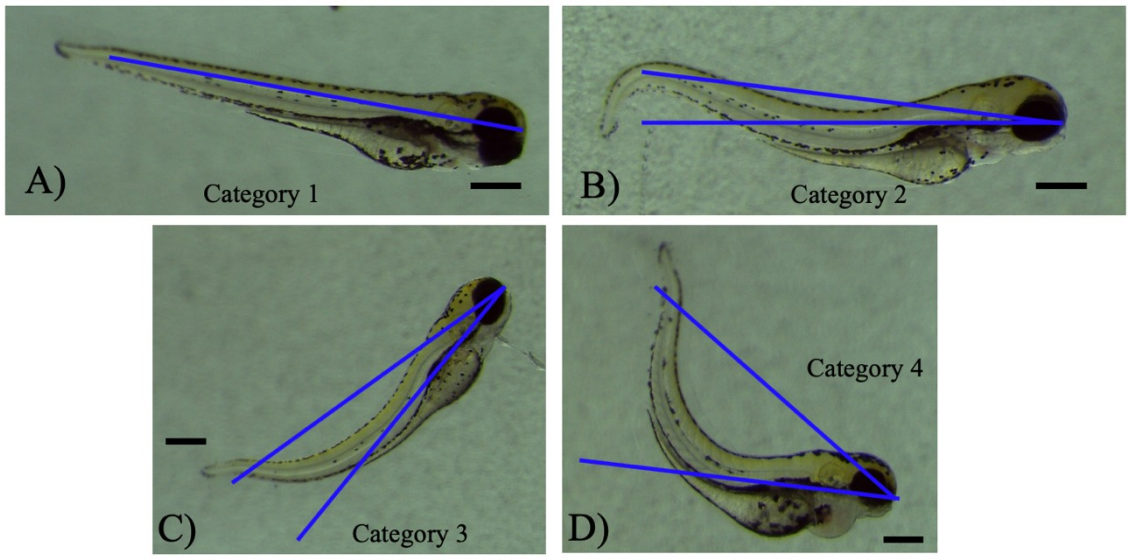

Figure 5. Lack of maternal contribution results in variable body axis defects

The offspring were separated into groups based on the type of bend seen. All the wild-type controls, along with 9.4% of *cep290* mutants fell into Category 1, which showed no bending (A). 62.5% of larvae fell into Category 2, showing a mild bend from 0.01° up to 10.00º, the offspring in this category was measured to be 7.68° (B). Category 3 displayed curves greater than 10.00º and under 30.00º, it held 15.6% of the analyzed mutants, the offspring shown was 15.31° (C). Curvatures more severe than 30.00° were placed under category 4, holding 12.5% of the mutants, the offspring shown was 32.70°. The scale bar represents 250 μm.

All of the wild-type embryos, and *cep290* mutants with heterozygous mothers, fell into category 1 with no abnormal curvatures present (Fig. 5.A). Table 5 sums up the parameters of each category along with the percentage of *cep290* mutant offspring that fell into each category.

Category	**Degree Range**	**% of *cep290* Mutant Offspring**
1	0.0°	9.4
2	0.01° - 10.00°	62.5
3	10.01° - 30.00°	15.6
4	>30.00°	12.5

Table 5: Percentage of mutant offspring in each category of curvatures

This experiment demonstrated that although maternal contribution of *cep290* is clearly important for early body axis establishment, there is considerable variation in this developmental event, suggesting a complex mechanism.

Adding to this suggestion of complexity, the two other zebrafish studies examining loss of *cep290* function in zebrafish also reported body axis curvature in larvae (Baye et al., 2011; Lessieur et al., 2019). However, the curvature reported by Baye and colleagues was ventral, with tail curved under the body, whereas the curvature reported by Lessieur et al, which notably occurred in less than 30% of larvae, was described as sigmoidal, or s-shaped. In contrast, the body axis curvatures noted here are mostly dorsal, curved toward the back.

3.4 A timeline of developmental requirements for Cep290 and Sans in body axis regulation

The important timepoints identified in this thesis and a previous lab student's thesis are summarized in the timeline (Fig. 6).

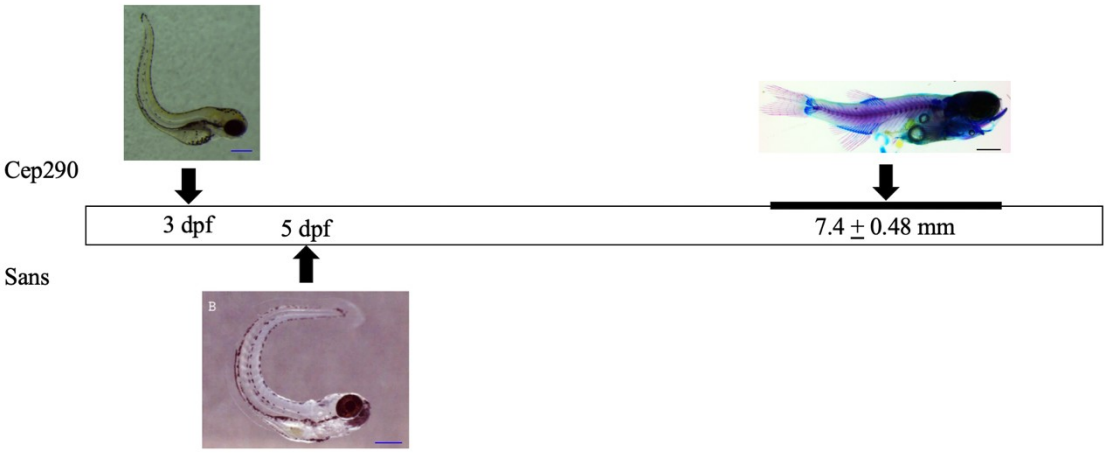

Figure 6. Cep290 and Sans importance in zebrafish body axis development

At 3 days post fertilization (dpf) and about when the fish reach 7.4 mm in standard length, the Cep290 protein is critical for body axis development and maintenance. Body axis curvature of in *sansa;sansb;cep290* triple mutants is seen at 5 dpf. The blue scale bar measures 250 μm, and the black scale bare measures 1 mm.

The *cep290* mutants lacking maternal *cep290* and the *sansa;sansb;cep290* mutants, shown at 3 and 5 days old respectively, have similar curvatures early in body axis development. By contrast, single *cep290* mutants from non-mutant mothers bypass the early Cep290 requirement for body axis development but exhibit defects later in larval development. Taken together, these findings support the hypothesis that the effect of *cep290* depletion on cilia-dependent body axis patterning is enhanced by the simultaneous absence of *sans* function. These results suggest that *cep290*, *sansa*, and *sansb* should be expressed in similar locations during zebrafish development. The Kupffer's vesicle (KV), a transient structure present during the period of embryonic development in which the zebrafish body axis is elongating (indicated in Figure 7), has well-studied roles in patterning growth and symmetry during this developmental stage.

3.5 *sansb* and *cep290* colocalize in the region of Kupffer's vesicle

The hypothesis that Sans interacts with Cep290 to regulate body axis development during early development suggests that *sans* genes should be present at a place and time consistent with this role. *cep290* expression in zebrafish was previously shown in the region of the KV (Baye et al., 2011). The KV is located on the ventral side of the embryo near the tail bud, and is present from 10 hpf until about 1 dpf. Because investigation of zebrafish *sans* was previously centered on its role in Usher syndrome, gene expression was visualized only within cells of the eyes and ears at later timepoints. Therefore, we tested whether *sans* transcripts could be detected in the KV.

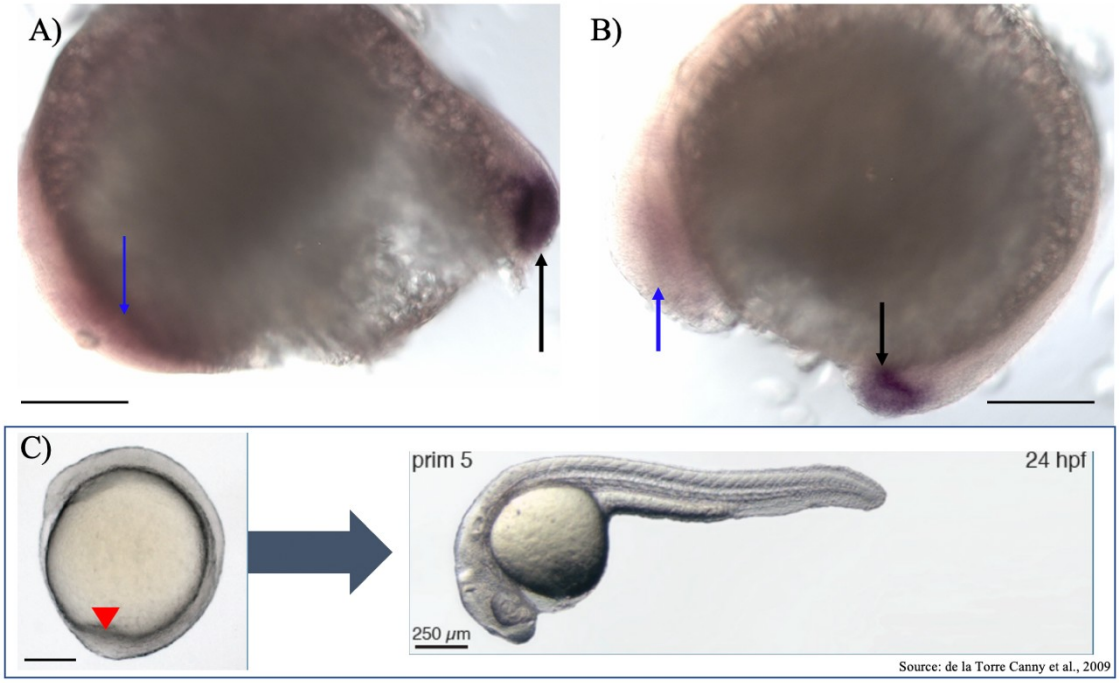

Figure 7: *sansb* and *cep290* are expressed in the tail bud proximal to the Kupffer's vesicle

In-situs were performed using a *sansb* (A) and a *cep290* (B) probe on wild-type embryos at 16 hpf to visualize the expression of the genes. In addition to faint expression in the head (blue arrow) both *sansb* and *cep290* transcripts are detected in the tail region near where the KV would be located (black arrow). The black scale bars represent 250 μm. Frame C shows the development of the body axis in zebrafish, in which the KV plays an important role. The KV is marked with a red arrowhead in a 10 hpf embryo and goes away around 24 hpf. (Source: de la Torre Canny et al., 2009)

sansb and *cep290* were both detected at 16 hpf, a timepoint approximately midway through the period in which the KV is active in body axis patterning. Both genes are expressed in a region proximal to the KV. This suggests a role for Sansb outside of the eyes and ears, which has not been identified previously.

The in-situs performed using a *sansa* probe were unsuccessful and could not be repeated due to the Covid-19 lab shutdown.

4. Conclusion and Discussion

This thesis sought to test the hypothesis that the effects of *cep290* depletion on cilia-dependent body axis patterning are enhanced by the simultaneous absence of *sans* function. As a prerequisite to this investigation, additional experiments were conducted to provide a baseline of *cep290* single mutant phenotypes and to characterize further the functionally redundant nature of the *sans* duplicates in zebrafish.

The first experiment described tested the genetic compensation question prompted by observations of *sansa* and *sansb* single mutants compared to *sansa;sansb* double mutants. RT-PCR on transcripts from embryos and larvae throughout the first week of development revealed the upregulation of *sansb* expression in *sansa* mutants, providing evidence that compensation by one gene, when the other genes is not functioning, is due to changes in gene regulation.

Next, experiments were conducted to characterize the phenotype of the *cep290* zebrafish mutation when isolated from the *sans* mutant background. Previous to the beginning of my thesis work, newly isolated *cep290* carriers were mated to determine whether the body axis curvature observed in *cep290;sans* mutant larvae was solely a result of the *cep290* mutation. None of the offspring of these crosses displayed an early curvature, but a spinal curvature was observed later in development in a subset of fish that were subsequently determined to be *cep290* mutants. To analyze this phenotype further, I conducted an experiment to identify the developmental stage at which the spinal curvature was first detectable, establishing a standard length measurement for this event. A timeline created by David Parichy provided a reference point for this developmental stage (Parichy et al., 2009). A figure in this publication depicting

increase in standard length plotted against time shows a steep slope during the third week of development, the period in which we observed the initiation of the spinal curvatures, indicating an accelerated growth period. This was of particular interest because of the comparative adolescent growth spurt in humans, which is when the onset of idiopathic scoliosis is most likely to occur.

My analysis established that the standard length when body axis curvature is first detectable occurs at 7.4 $\pm$ 0.48 mm. These curvatures were further visualized using a double stain and compared to stage-matched wild-type controls. Multiple regions of spinal curvature were observed including both dorsoventral and lateral displacements. All of the fish that displayed this curvature were identified as *cep290* mutants by sequence analysis, fish that did not display curvatures were either wild-type or heterozygous for *cep290*. This phenotype is similar to that reported in the investigation of *cep290* mutants that was published during my thesis research (Lessieur et al., 2019). These results indicate that *cep290* mutations cause a disruption in the flow of CSF, presumably, by impairing the function of the cilia involved in body axis development.

When *sans* genes are functional, *cep290* mutants survive past the early curvature timepoint and exhibit the delayed spinal curvature. We hypothesized that the unremarkable early development of *cep290* mutants was due to the maternal genotype. To test for this maternal effect, embryos from homozygous *cep290* mutant mothers were procured and compared to embryos from heterozygous *cep290* mothers. The offspring of the *cep290* mutant mothers exhibited curvatures by 3 days old, whereas the offspring of the heterozygous *cep290* mothers did not. This result indicated that maternally contributed Cep290 is active during embryonic body axis development. The

previous finding that a similar curvature, presumed to be the result of dysfunctional ciliary movement, manifests in *sans;cep290* mutants in this early time period suggested that Sans may be playing a role in cilia function beyond the retina, in concert with Cep290. In-situ hybridizations were performed on wild-type embryos at 16 hpf to learn whether the two genes were expressed in the KV, a ciliated structure known to be involved in body axis establishment during embryogenesis and where *cep290* has been previously found to localize. *sansb* and *cep290* transcripts were both detected in cells proximal to the KV, consistent with the hypothesis that Sansb and Cep290 are interacting in this process. The late larval body axis curvature observed in *cep290* mutants with heterozygous *cep290* mothers was similar to the phenotype observed in a study of zebrafish models of idiopathic scoliosis (Grimes et al., 2016). The phenotype reported in this study was thought to be a result of dysfunctional motile cilia involved in the flow of cerebrospinal fluid (CSF). The similarity in body axis disfigurements of the zebrafish in this thesis compared to that of Grimes and colleagues provides further support for our conclusion that *cep290* is important for the function of the motile cilia responsible for the flow of CSF in zebrafish.

My hypothesis, which states that the effect of *cep290* depletion on cilia-dependent body axis patterning is enhanced by the simultaneous absence of *sans* function, is supported by the data presented in this thesis. The results from the in-situ hybridization experiments and the early curvature seen at 5 dpf in *sans;cep290* mutants which is not seen in *cep290* mutants with heterozygous mothers are consistent with an enhanced disruption of the body axis development due to an interaction between Sans and Cep290.

5. Future Studies

This thesis provides a baseline phenotype for the *cep290* mutation, showing a delayed scoliosis phenotype at 7.4 ± 0.48 mm standard length and an early body axis curvature by 3 days old dependent on the maternal genotype. This thesis also provides insight into how the two orthologs of human *SANS* found in zebrafish, *sansa* and *sansb*, can compensate for each other if one of them is non-functional. Furthermore, we observed that *sansb* and *cep290* are both expressed in the KV, which, in addition to providing the first evidence of *sans* expression outside the visual and auditory sensory cells, supports the hypothesis that *sans* and *cep290* interact during the development of the body axis.

The reciprocal RT-PCR experiment should be done to see whether *sansa* transcription is upregulated in the *sansb* mutant. The expected result, consistent with the lack of phenotype in single mutants, is an increase in *sansa* expression.

The expression patterns of *sans* and *cep290* should be further characterized by performing in-situ hybridizations in wild-type fish at expanded timepoints within and before the interval that the KV is present and actively patterning the body axis. Additional timepoint analysis could establish a critical period for the hypothesized interaction between Sans and Cep290 in body axis patterning circa the KV, and also determine whether *cep290* and *sans* have any other areas with common expression, which could indicate additional interactions in other tissues. Furthermore, an in situ with a *sansa* probe should be conducted to assay the expression in the KV.

The expression of genes dependent on proper CSF flow should also be analyzed by in-situ hybridizations on *cep290* mutants, *sans* mutants, and *cep290;sans* mutants.

The fluid flow that patterns the body axis and symmetry activates a variety of downstream targets with further roles in embryonic development. Evaluating how the expression of these downstream factors is affected by the loss of *sans* and *cep290* function will further identify the mechanism by which the combinations of mutants in this study cause body axis curvatures through cilia dysfunction. These experiments will help to characterize further the functions of the proteins as well as their partnership.

Acetylated tubulin is a protein subunit of microtubules, which make up cilia. Antibodies can be used to label acetylated tubulin in zebrafish cells. Antibody staining of acetylated tubulin should be performed on the motile cilia, including Kupffer's vesicle (KV) and the cilia in the spinal cord that regulate CSF flow later in development. Visualizing these structures in *sans* mutants, *cep290* mutants, and *sans;cep290* mutants compared to wild type would determine how each mutation or combination of mutations affected the formation of these cilia, a necessary step to determine whether the defects observed in these mutants are based on improper cilia formation or function.

Zebrafish have pigment spots that contain melanosomes that expand or contract in response to environmental light levels. The process of expanding and contracting the melanosomes is a microtubule based system. Therefore, melanosome transport is a readout of microtubule transport. Defective melanosome transport was reported in the previous study of loss of *cep290* function in zebrafish (Baye et al., 2011) so it would be informative to analyze this process in *sans* mutants, *cep290* mutants, and *sans;cep290* mutants. If dysfunction in melanosome transport is observed, this would further clarify the interaction between *cep290* and *sans* as it relates to microtubule function.

This thesis project has set up the next steps in validating the Sans-Cep290 interaction in zebrafish. The discovery of this interaction creates a better understanding of how Cep290 functions in zebrafish. The validation of this interaction would implicate a role for Sans outside of the visual and auditory systems, and its possible function in body axis maintenance, which, when disrupted, can result in scoliosis. If the function of Sans outside of USH systems were confirmed, it would call to question the functions of other USH genes, leading to a new course of research to implicate them in other disorders and interactions they may have. This information would be useful for generating improved clinical tools such as gene therapies. The results described in this thesis are part of a global research effort to enhance our collective understanding of the genetic variations that influence virtually every aspect of human life.

Bibliography

Baschal, E. E., Terhune, E. A., Wethey, C. I., Baschal, R. M., Robinson, K. D., Cuevas, M. T., ... & Pearson, C. G. (2018). Idiopathic Scoliosis Families Highlight Actin-Based and Microtubule-Based Cellular Projections and Extracellular Matrix in Disease Etiology. *G3: Genes, Genomes, Genetics*, *8*(8), 2663-2672.

Baye, L. M., Patrinostro, X., Swaminathan, S., Beck, J. S., Zhang, Y., Stone, E. M., ... & Slusarski, D. C. (2011). The N-terminal region of centrosomal protein 290 (CEP290) restores vision in a zebrafish model of human blindness. *Human molecular genetics*, *20*(8), 1467-1477.

Bensimon-Brito, A., Cardeira, J., Cancela, M. L., Huysseune, A., & Witten, P. E. (2012). Distinct patterns of notochord mineralization in zebrafish coincide with the localization of Osteocalcin isoform 1 during early vertebral centra formation. *BMC developmental biology*, *12*(1), 28.

Chang, B., Khanna, H., Hawes, N., Jimeno, D., He, S., Lillo, C., ... & Sayer, J. A. (2006). In-frame deletion in a novel centrosomal/ciliary protein CEP290/NPHP6 perturbs its interaction with RPGR and results in early-onset retinal degeneration in the rd16 mouse. *Human molecular genetics*, *15*(11), 1847-1857.

Coppieters, F., Lefever, S., Leroy, B. P., & De Baere, E. (2010). CEP290, a gene with many faces: mutation overview and presentation of CEP290base. *Human mutation*, *31*(10), 1097-1108.

Craige, B., Tsao, C. C., Diener, D. R., Hou, Y., Lechtreck, K. F., Rosenbaum, J. L., & Witman, G. B. (2010). CEP290 tethers flagellar transition zone microtubules to the membrane and regulates flagellar protein content. *Journal of Cell Biology*, *190*(5), 927-940.

Dad, S., Østergaard, E., Thykjaer, T., Albrectsen, A., Ravn, K., Rosenberg, T., & Møller, L. B. (2010). Identification of a novel locus for a USH3 like syndrome combined with congenital cataract. *Clinical genetics*, *78*(4), 388-397.

de la Torre Canny, S. G., Holterhoff, C., Behringer, R., Wagner, D., & Kozlowski, D. (2009). Go Fish!. *Genesis*, *47*.

den Hollander, A. I., Roepman, R., Koenekoop, R. K., & Cremers, F. P. (2008). Leber congenital amaurosis: genes, proteins and disease mechanisms. *Progress in retinal and eye research*, *27*(4), 391-419.

Dona, M., Slijkerman, R., Lerner, K., Broekman, S., Wegner, J., Howat, T., Peters, T., Hetterschijt, L., Boon, N., de Vrienze, E., Sorusch, N., Wolfrum, U., Kremer, H., Neuhauss, S., Zang, J., Kamermans, M., Westerfield, M., Phillips, J., van Wijk, E. (2018). Usherin defects lead to early-onset retinal dysfunction in zebrafish. *Experimental eye research*, *173*, 148-159.

Espinos, C., Najera, C., Millan, J. M., Ayuso, C., Baiget, M., Perez-Garrigues, H., ... & Beneyto, M. (1998). Linkage analysis in Usher syndrome type I (USH1) families from Spain. *Journal of medical genetics*, *35*(5), 391-398.

Fliegauf, M., Benzing, T., & Omran, H. (2007). When cilia go bad: cilia defects and ciliopathies. *Nature reviews Molecular cell biology*, *8*(11), 880-893.

Force, A., Lynch, M., Pickett, F. B., Amores, A., Yan, Y. L., & Postlethwait, J. (1999). Preservation of duplicate genes by complementary, degenerative mutations. *Genetics*, *151*(4), 1531-1545.

Frank, V., den Hollander, A. I., Brüchle, N. O., Zonneveld, M. N., Nürnberg, G., Becker, C., ... & Nürnberg, P. (2008). Mutations of the CEP290 gene encoding a centrosomal protein cause Meckel Gruber syndrome. *Human mutation*, *29*(1), 45-52.

Grimes, D. T., Boswell, C. W., Morante, N. F. C., Henkelman, R. M., Burdine, R. D., & Ciruna, B. (2016). Zebrafish models of idiopathic scoliosis link cerebrospinal fluid flow defects to spine curvature. *Science*, *352*(6291), 1341-1344.

Hayes, M., Gao, X., Lisa, X. Y., Paria, N., Henkelman, R. M., Wise, C. A., & Ciruna, B. (2014). ptk7 mutant zebrafish models of congenital and idiopathic scoliosis implicate dysregulated Wnt signalling in disease. *Nature communications*, *5*(1), 1-11.

Hirokawa, N., Tanaka, Y., Okada, Y., & Takeda, S. (2006). Nodal flow and the generation of left-right asymmetry. *Cell*, *125*(1), 33-45.

Howe, K., Clark, M. D., Torroja, C. F., Torrance, J., Berthelot, C., Muffato, M., ... & McLaren, S. (2013). The zebrafish reference genome sequence and its relationship to the human genome. *Nature*, *496*(7446), 498-503.

Kimberling, W. J., Hildebrand, M. S., Shearer, A. E., Jensen, M. L., Halder, J. A., Trzupek, K., Cohn, E. S., Weleber, R. G., Stone, E. M., & Smith R. J. (2010). Frequency of Usher syndrome in two pediatiric populations: Implications for genetic screening of deaf and hard of hearing children. *Genetics in Medicine*, *12*(8), 512-516.

Kremer, H., van Wijk, E., Märker, T., Wolfrum, U., & Roepman, R., (2006). Usher syndrome: molecular links of pathogenesis, proteins and pathways. *Human molecular genetics*, *15*(suppl_2), R262-R270.

Lessieur, E. M., Song, P., Nivar, G. C., Piccillo, E. M., Fogerty, J., Rozic, R., & Perkins, B. D. (2019). Ciliary genes arl13b, ahi1 and cc2d2a differentially modify expression of visual acuity phenotypes but do not enhance retinal degeneration due to mutation of cep290 in zebrafish. *PloS one*, *14*(4).

Mathur, P., & Yang, J. (2015). Usher syndrome: hearing loss, retinal degeneration and associated abnormalities. *Biochimica et Biophysica Acta (BBA)-Molecular Basis of Disease*, *1852*(3), 406-420.

Okada, Y., Takeda, S., Tanaka, Y., Belmonte, J. C. I., & Hirokawa, N. (2005). Mechanism of nodal flow: a conserved symmetry breaking event in left-right axis determination. *Cell*, *121*(4), 633-644.

Parichy, D. M., Elizondo, M. R., Mills, M. G., Gordon, T. N., & Engeszer, R. E. (2009). Normal table of postembryonic zebrafish development: staging by externally visible anatomy of the living fish. *Developmental dynamics*, *238*(12), 2975-3015.

Phillips, J. B., & Westerfield, M. (2014). Zebrafish models in translational research: tipping the scales toward advancements in human health. *Disease models & mechanisms*, *7*(7), 739-743.

Phillips, J. B., Blanco-Sanchez, B., Lentz, J. J., Tallafuss, A., Khanobdee, K., Sampath, S., ... & Williams, D. S. (2011). Harmonin (Ush1c) is required in zebrafish Müller glial cells for photoreceptor synaptic development and function. *Disease models & mechanisms*, *4*(6), 786-800.

Phillips, J. B., Wegner, J., & Westerfield, M. (2015). Duplicated zebrafish orthologs of USH1G have partially overlapping function in sensory cells. *Investigative Ophthalmology & Visual Science*, *56*(7), 5994-5994.

Reiners, J., Nagel-Wolfrum, K., Jürgens, K., Märker, T., & Wolfrum, U. (2006). Molecular basis of human Usher syndrome: deciphering the meshes of the Usher protein network provides insights into the pathomechanisms of the Usher disease. *Experimental eye research*, *83*(1), 97-119.

Reisser, C. F., Kimberling, W. J., & Otterstedde, C. R. (2002). Hearing loss in Usher syndrome type II is nonprogressive. *Annals of Otology, Rhinology & Laryngology*, *111*(12), 1108-1111.

Reiter, J. F., & Leroux, M. R. (2017). Genes and molecular pathways underpinning ciliopathies. *Nature reviews Molecular cell biology*, *18*(9), 533.

Seiler, C., Finger-Baier, K. C., Rinner, O., Makhankov, Y. V., Schwarz, H., Neuhauss, S. C., & Nicolson, T. (2005). Duplicated genes with split functions: independent roles of protocadherin15 orthologues in zebrafish hearing and vision. *Development*, *132*(3), 615-623.

Söllner, C., Rauch, G. J., Siemens, J., Geisler, R., Schuster, S. C., Müller, U., & Nicolson, T. (2004). Mutations in cadherin 23 affect tip links in zebrafish sensory hair cells. *Nature*, *428*(6986), 955-959.

Sorusch, N., Wunderlich, K., Bauss, K., Nagel-Wolfrum, K., & Wolfrum, U. (2014). Usher syndrome protein network functions in the retina and their relation to other retinal ciliopathies. In *Retinal Degenerative Diseases* (pp. 527-533). Springer, New York, NY.

Valente, E. M., Silhavy, J. L., Brancati, F., Barrano, G., Krishnaswami, S. R., Castori, M., ... & Fazzi, E. (2006). Mutations in CEP290, which encodes a centrosomal protein, cause pleiotropic forms of Joubert syndrome. *Nature genetics*, *38*(6), 623-625.

Weil, D., El-Amraoui, A., Masmoudi, S., Mustapha, M., Kikkawa, Y., Lainé, S., ... & Hamel, C. (2003). Usher syndrome type IG (USH1G) is caused by mutations in the gene encoding SANS, a protein that associates with the USH1C protein, harmonin. *Human molecular genetics*, *12*(5), 463-471.

White, R. M., Cech, J., Ratanasirintrawoot, S., Lin, C. Y., Rahl, P. B., Burke, C. J., ... & Chen, F. (2011). DHODH modulates transcriptional elongation in the neural crest and melanoma. *Nature*, *471*(7339), 518-522.

Wolfrum, U., Sorusch, N., Knapp, B., Janson, J., Fleck, W. D., & Scharf, C. (2019). SANS (USH1G) molecularly links the human Usher syndrome protein network to the intraflagellar transport module by direct binding to IFT-B proteins. *Frontiers in cell and developmental biology*, *7*, 216.

Yan, J., Pan, L., Chen, X., Wu, L., & Zhang, M. (2010). The structure of the harmonin/sans complex reveals an unexpected interaction mode of the two Usher syndrome proteins. *Proceedings of the National Academy of Sciences*, *107*(9), 4040-4045.

Zaghloul, N. A., & Katsanis, N. (2011). Zebrafish assays of ciliopathies. In *Methods in cell biology* (Vol. 105, pp. 257-272). Academic Press.